Journal of Translational Medicine

RESEARCH

Open Access

H2BC9 lactylation modulates esophageal squamous cell carcinoma progression via the Wnt/β-catenin signaling pathway

Yuxiang Zhang[1†], Ce Shi[1,4†], Yun Zhou[5†], Jing Zhu[1], Keke Xia[3], Lin Wang[1], Shuling Wang[6], Jie Mou[3*], Lansheng Zhang[2*] and Dongsheng Pei[1*]

Abstract

Background Lactate, traditionally regarded as a metabolic waste product of glycolysis, has recently emerged as a critical signaling molecule and epigenetic modifier via protein lactylation. However, the functional consequences of histone lactylation in cancer progression remain poorly understood.

Methods We integrated transcriptomic data from TCGA and GEO (GSE188900) with bulk and single-cell RNA-seq analyses to identify lactylation-associated histone variants involved in esophageal squamous cell carcinoma (ESCC). Functional assays, immunoprecipitation (IP), western blotting (WB), chromatin immunoprecipitation (ChIP)-qPCR, and luciferase reporter assays were employed to investigate the role of H2BC9 and its lactylation in ESCC. A xenograft tumor model was used to validate in vivo relevance.

Results We identified H2BC9, a histone H2B variant, as a lactylation-associated oncogene that is overexpressed in ESCC and correlates with poor prognosis. Lactate stimulation induced H2BC9 lactylation, particularly at lysine 44 (K44), as confirmed by mass spectrometry and IP-WB assays. Mechanistically, K44 lactylation of H2BC9 enhanced the transcriptional activity of Wnt7b, leading to activation of the Wnt/β-catenin pathway. Mutation of K44 (K44R) abolished H2BC9 lactylation and significantly impaired its ability to promote ESCC cell proliferation and Wnt7b transcription, as demonstrated by ChIP-qPCR and dual-luciferase assays. In vivo, H2BC9 K44R-expressing cells exhibited reduced tumor growth in xenograft models. Furthermore, H2BC9 expression was associated with an immunosuppressive tumor microenvironment and chemoresistance.

†Yuxiang Zhang, Ce Shi, Yun Zhou have contributed equally to this work.

*Correspondence:
Jie Mou
mou.jie@xzhmu.edu.cn
Lansheng Zhang
lanshengyan@163.com
Dongsheng Pei
dspei@xzhmu.edu.cn

Full list of author information is available at the end of the article

Conclusion Our study reveals a novel regulatory axis in which H2BC9 K44 lactylation activates Wnt7b transcription and downstream Wnt/β-catenin signaling, driving ESCC progression. Targeting H2BC9 lactylation may offer a promising therapeutic strategy to overcome tumor growth and immune evasion in ESCC.

Keywords Esophageal squamous cell carcinoma (ESCC), Lactylation, H2BC9, Wnt/β-catenin signaling pathway

Introduction

Esophageal cancer (EC) remains a significant global health burden, with 510,716 new cases and 445,129 deaths reported in 2022 according to the Global Cancer Observatory (GLOBOCAN) [1, 2]. In the Chinese population, esophageal squamous cell carcinoma (ESCC) accounts for more than 90% of all EC cases [3]. Despite advances in diagnosis and treatment over the past decades, the 5-year survival rate of EC remains below 30%, and its underlying molecular mechanisms are still not fully understood [4].

Among the hallmarks of cancer, aberrant metabolism has emerged as a key contributor to tumor progression [5, 6]. One of the most well-characterized metabolic alterations in cancer is the Warburg effect, which describes the preference of tumor cells for glycolysis even in the presence of oxygen [7]. Tumor cells exhibit enhanced glycolytic activity, converting glucose to lactate even under normoxic conditions—a phenomenon that distinguishes them from normal cells [8–10]. Traditionally, lactate was regarded merely as a metabolic byproduct [11, 12]. However, emerging evidence suggests that lactate functions not only as a metabolic substrate but also as a signaling molecule involved in diverse cellular processes [13]. Notably, in 2019, lactate was identified as a donor for lysine lactylation, a novel post-translational modification with regulatory potential [13, 14]. However, the biological functions and regulatory mechanisms of protein lactylation in cancer remain largely unexplored.

H2BC9 is a member of the histone H2B family and a variant of the core histone H2B, involved in nucleosome assembly and chromatin stabilization [15]. Structurally, it contains a highly conserved H2B-fold domain that enables the formation of histone octamers with H2A, H3, and H4, thereby regulating DNA packaging and transcriptional activity [16, 17]. H2BC9 plays a critical role in epigenetic regulation, participating in chromatin remodeling, DNA repair, and gene expression [18]. In various cancers, upregulation of H2BC9 has been associated with abnormal cell proliferation, increased invasiveness, and poor prognosis, suggesting that it may promote tumorigenesis by modulating chromatin accessibility and transcriptional programs [19]. However, most histone-related studies have focused on the H3 family, and the biological functions of H2B variants, including H2BC9, remain poorly understood [20, 21]. To date, the lactylation of H2BC9 and its potential biological implications have not been reported.

Here, we demonstrate that histone lactylation plays a crucial role in the progression of ESCC. Mechanistically, H2BC9 undergoes lactylation at lysine 44 in response to elevated lactate levels in the tumor microenvironment. This modification facilitates transcriptional activation of the Wnt/β-catenin signaling pathway, notably through upregulation of Wnt7b. Functionally, H2BC9 lactylation promotes tumor cell proliferation, cell cycle progression, and immune evasion. Mutation of the K44 site abrogates these effects, highlighting its regulatory specificity. In vivo xenograft models and clinical tissue analysis further corroborate the oncogenic role of H2BC9 lactylation. Collectively, our findings uncover a novel epigenetic mechanism by which lactylation of H2BC9 drives ESCC progression, and propose H2BC9 as a potential biomarker and therapeutic target.

Materials and methods

Bulk RNA-seq datasets

The bulk RNA-seq data of ESCC and their corresponding phenotype data were downloaded from the TCGA database, while the bulk RNA-seq data of normal esophageal tissues and their phenotype data were obtained from the GTEx database. The sequencing data were in FPKM format and were log2(fpkm + 1) transformed. Batch effects were removed using the ComBat function from the "sva" (v 3.20.0) package.

ScRNA-seq datasets

The GSE188900 dataset was obtained from the Gene Expression Omnibus (GEO) database. This dataset was submitted in 2021 and publicly released in 2022. It was generated using the Illumina NovaSeq 6000 platform (GPL24676), and contains single-cell RNA sequencing data from 7 tumor tissues and 1 adjacent non-tumor tissue derived from 5 patients with ESCC.

In the present study, we utilized sequencing data from the 7 tumor tissue samples. Quality control and downstream analyses were performed using the Seurat package. Low-quality cells or empty droplets with fewer than 200 detected genes, as well as doublets or multiplets with more than 5000 detected genes, were excluded. Additionally, cells with high mitochondrial gene content (> 10%) were considered low-quality or dying and were removed. Batch effect correction across patient samples was conducted using the Harmony package. Highly variable genes were identified following standard procedures, and

data normalization was subsequently performed based on these genes.

Gene set variation analysis (GSVA)

GSVA is a method employed to assess the variation in gene set activity across different samples. This approach reflects the activity differences of a gene set under various biological states by calculating the degree of variation for specific gene sets in each sample. In this study, glycolysis-related and lactate-related gene sets were collected from the MSigDB database, and scores were generated and visualized for tumor samples and normal tissues [22].

Differential gene expression analysis

The "limma" (v3.54.0) package was utilized for differential gene expression analysis. It is a widely used R package for both microarray and RNA-seq differential analysis, providing robust linear model fitting capabilities to effectively handle complex experimental designs and data structures. Differentially expressed genes between tumor tissues and normal tissues were identified based on the criteria of $|\log2FC| > 2$ and a false discovery rate (FDR) < 0.05. For the epithelial cell subpopulations in single-cell data, differential analysis was performed with the threshold of $|\log2FC| > 1$ and FDR < 0.05.

Obtain of lactate-related genes

The GeneCards database was queried using " **lactate** " as the keyword, and the results were filtered to include only protein-coding genes. A total of 115 related genes were identified [23].

Random forest model

Random forest, a decision tree-based machine learning algorithm, was employed to assess the contribution of variables to heterogeneity. In this study, random forest was utilized to identify lactate-related genes with heterogeneous expression between tumor and normal tissues.

Survival analysis and clinical correlation analysis

Survival data and phenotype information of ESCC patients were downloaded from the TCGA database. The "survival" (v3.6–4) and "survminer" (v0.4.9) packages were utilized for survival analysis and visualization of Kaplan–Meier (KM) curves. The "rms"(v6.8–2) package was applied to fit regression models and construct a nomogram based on the Cox proportional hazards model. Calibration curves were generated using bootstrap resampling to assess the accuracy of the Cox regression model.

Protein–protein interaction (PPI) analysis

PPI networks were analyzed using the STRING database, and the results were exported. The interaction data were then refined and visualized using Cytoscape software to enhance the presentation of the network.

Gene set enrichment analysis (GSEA)

To explore the biological functions and signaling pathways of differentially expressed genes, enrichment analysis was performed using the Gene Ontology (GO) and Kyoto Encyclopedia of Genes and Genomes (KEGG) databases. The "clusterProfiler" (v4.8.2) package was employed for enrichment analysis, with a significance threshold of P-value < 0.05. The Benjamini–Hochberg method was applied to adjust for multiple testing, allowing the identification and visualization of significantly enriched pathways among the differentially expressed genes.

Prediction of drug sensitivity

Drug sensitivity prediction was conducted using the "OncoPredict" (v 1.2) package. Bulk RNA-seq data for ESCC were standardized to ensure data consistency. Drug sensitivity scores were then calculated by the OncoPredict algorithm based on the gene expression profiles of drug targets, reflecting the responsiveness of different samples to various drugs. Results with a P-value < 0.05 were considered statistically significant.

Analysis of somatic mutations

Somatic mutation analysis was conducted using the "maftools" (v 2.20.0) package. First, mutation data were obtained from TCGA and converted into Mutation Annotation Format (MAF). The mutation data were then imported using the read.maf function, and an overview of mutation frequencies and types was generated with the plotmafSummary function. Key driver gene mutations were visualized using functions such as oncoplot and lollipopPlot. To compare mutation differences between groups, the mafCompare function was employed. Additionally, the somaticInteractions function was used to assess co-mutation relationships between genes, providing further insight into their potential biological significance. The cBioPortal database was used for the analysis of mutation abundance of H2BC9.

Immune infiltration analysis

Immune infiltration was analyzed using CIBERSORT and ssGSEA. Bulk RNA-seq data from TCGA were processed using CIBERSORT with the LM22 signature matrix (1000 permutations), selecting samples with $P < 0.05$. And ssGSEA was performed via the GSVA R package, using immune-related gene sets from MSigDB to quantify immune cell enrichment. Statistical comparisons were conducted using the Wilcoxon rank-sum test, and correlations were assessed via Spearman's method. Data visualization included heatmaps, boxplots, and correlation

matrices, with all analyses performed in R. Statistical significance was set at $P < 0.05$.

CellChat

The "CellChat" (v1.6.1) package was employed to quantitatively infer and analyze intercellular communication networks across different cell types. CellChat accurately represents known heteromeric molecular complexes, constructing a comprehensive database of interactions among ligands, receptors, and their cofactors. Based on the law of mass action, CellChat predicts the primary signaling inputs and outputs of cells and uses network analysis and pattern recognition methods to examine how intercellular signals are coordinated to achieve functional outcomes. This approach unveils the dynamics of cell communication and its potential roles in biological functions.

Western blotting (WB)

Cells or tissue samples were lysed in RIPA buffer (Beyotime, China) supplemented with protease and phosphatase inhibitors (Beyotime, China) and incubated on ice for 15 min. The lysates were centrifuged at 12,000 × g for 15 min at 4 °C, and the supernatants were collected for protein quantification using the BCA protein assay kit (Beyotime, China). Equal amounts of protein were separated by SDS-PAGE on 4–20% polyacrylamide gels and transferred onto NC membranes (Millipore, USA) at 300 mA for 40 min. Membranes were blocked with 5% non-fat milk in TBST (TBS containing 0.1% Tween-20) for 1 h at room temperature and incubated overnight at 4 °C with primary antibodies (Supplementary Table 1). After washing three times with TBST, membranes were incubated with HRP-conjugated secondary antibodies (1:5000) for 1 h at room temperature. Protein bands were visualized using an enhanced chemiluminescence (ECL) detection kit (Bio-Rad, USA) and imaged with a chemiluminescent imaging system (ChemiDoc MP, Bio-Rad).

Immunoprecipitation (IP)

Cells were lysed in lysis buffer (50 mM Tris–HCl, 150 mM NaCl, 1% NP-40, pH 7.5) supplemented with protease inhibitors on ice for 30 min. Lysates were cleared by centrifugation at 12,000 × g for 10 min at 4 °C. Supernatants were incubated with primary antibody or isotype control IgG at 4 °C overnight, followed by the addition of Protein A/G agarose beads for 2 h (Supplementary Table 1). After washing three times with lysis buffer, immune complexes were eluted with SDS sample buffer and analyzed by WB.

Cell proliferation assay (CCK-8)

Cell viability was assessed using the Cell Counting Kit-8 (Beyotime, China) according to the manufacturer's instructions. Cells were seeded in 96-well plates at a density of 2000 cells/well and cultured for 24 h. At the indicated time points, 10 μL of CCK-8 solution was added to each well and incubated at 37 °C for 1 h. Absorbance was measured at 450 nm using a microplate reader (Thermo Fisher, USA). Each experiment was performed in triplicate.

Colony formation assay

Cells were seeded in 6-well plates at a density of 300 cells per well and cultured in complete medium for 14 days until visible colonies formed. The medium was replaced every 3 days. Colonies were fixed with 4% paraformaldehyde for 15 min and stained with 0.1% crystal violet for 30 min. After washing with distilled water, colonies containing more than 50 cells were counted under a microscope. Each experiment was performed in triplicate to ensure reproducibility.

Prediction of lactylation sites

DeepKla was utilized to predict potential lactylation sites on proteins, employing a deep learning model. By integrating embedding layers, convolutional neural networks, bidirectional gated recurrent units, and attention mechanisms, DeepKla effectively predicts lactylation modification sites, demonstrating exceptional predictive power and robustness. FSL-Kla is a multi-feature hybrid system based on Few-Shot Learning (FSL) designed to predict lysine lactylation (Kla) sites in proteins. By integrating multiple features and leveraging a limited number of known Kla site data, this tool constructs an efficient predictive model.

Mass spectrometry

TE-1 cells treated with 20 mM lactate for 24 h were lysed and digested with trypsin. The resulting peptides were enriched for lactylated peptides using anti-lactyl-lysine antibodies (PTM Bio, China). Enriched peptides were analyzed by liquid chromatography-tandem mass spectrometry (LC–MS/MS) on a Q Exactive mass spectrometer (Thermo Fisher, USA). The raw data were processed with MaxQuant software (version v2.2.0.0) to identify and quantify lactylation sites on H2BC9 protein.

Dual-luciferase reporter assay

TE-1 and EC109 cells were seeded in 24-well plates and co-transfected with a Wnt7b promoter-driven firefly luciferase reporter plasmid (pGL3-Wnt7b) and a Renilla luciferase control plasmid (pRL-TK) using Lipofectamine 3000 (Invitrogen, USA). After 24 h of transfection, cells were treated with 20 μM lactate for 24 h to induce lactylation of H2BC9. Cell lysates were prepared and luciferase activity was measured using the Dual-Luciferase Reporter Assay System (Promega, USA) according to the

manufacturer's instructions. The firefly luciferase activity was normalized to Renilla luciferase activity to account for transfection efficiency. All experiments were performed in triplicate, and the relative luciferase activity was compared between treated and untreated groups to evaluate the effect of H2BC9 lactylation on Wnt7b transcriptional activation.

Chromatin immunoprecipitation (ChIP) and qPCR

ChIP assays were conducted using the SimpleChIP® Enzymatic Chromatin IP Kit (CST, #9003) according to the manufacturer's instructions. TE-1 cells were cross-linked with 1% formaldehyde, quenched with glycine, and chromatin was digested with micrococcal nuclease followed by sonication. IP was performed overnight at 4 °C using antibodies against H2BC9 and control IgG.

DNA was purified and analyzed by qPCR using SYBR Green Master Mix (Vazyme, #Q711-02). Enrichment was calculated as % input:

$$\%\,\mathrm{Input} = 2^{[ct(\mathrm{Input}) - ct(\mathrm{IP})]} * 100\%$$

In vivo mouse studies

All animal experiments were approved by the Experimental Animal Ethics Committee of Xuzhou Medical University (Approval No. 202507T011) and conducted in accordance with institutional guidelines for animal welfare. Female BALB/c nude mice were purchased from Jiangsu GemPharmatech Co., Ltd. and housed under pathogen-free conditions.

TE-1 cells stably transduced with either wild-type (WT) H2BC9, K44R mutant H2BC9, or corresponding controls (sgNC, sgH2BC9) were harvested and resuspended in 100 μL PBS. A total of 5×10^6 cells were subcutaneously injected into the right flanks of the mice (n = 5 per group). Tumor volume was measured with digital calipers every three days, and calculated using the formula:

$$\mathrm{Volume} = \left(\mathrm{Length} \times \mathrm{Width}^2\right) \times 0.5$$

At 21 days post-inoculation, or when tumors approached the ethical endpoint (~ 1000 mm^3), mice were euthanized via CO_2 inhalation. Tumors were excised, photographed, and weighed. All procedures were performed under sterile conditions to ensure animal welfare and data reliability.

Results

H2BC9 is identified as an oncogene related to lactate in ESCC

The Warburg effect, characterized by enhanced aerobic glycolysis, represents a critical hallmark of tumor metabolism and plays a key role in cancer progression. In ESCC, Gene Set Variation Analysis (GSVA) identified significant enrichment of glycolysis- and lactate-related gene sets in tumor cells, underlining the importance of metabolic reprogramming in tumorigenesis (Fig. 1a). Differential expression analysis between normal and ESCC cells revealed 844 upregulated and 1,067 downregulated genes (|log2FC| > 2, *P*.adj < 0.05) (Fig. 1b). Univariate Cox regression analysis highlighted the top five prognostic genes, which were visualized in a forest plot (Fig. 1c). Targeting " **lactate**," 115 related genes were extracted from GeneCards, with 10 selected for heatmap visualization, showcasing expression patterns relevant to ESCC (Fig. 1d). A random forest algorithm further prioritized 20 key genes, leading to the identification of H2BC9 as a pivotal molecular candidate (Fig. 1e). This integrative analytical approach underscores H2BC9's potential role in driving ESCC pathogenesis and sets the stage for deeper mechanistic and therapeutic investigations (Fig. 1f).

H2BC9 is highly expressed in various tumors and is associated with poor prognosis in ESCC patients

Analysis of sequencing data from TCGA and microarray data from the GEO database revealed that H2BC9 is highly expressed in ESCC tumor tissues (Fig. 2a and b). Additionally, WB indicated that the expression level of H2BC9 was elevated in ESCC cell lines compared to normal esophageal epithelial cells (Fig. 2c). Furthermore, elevated expression of H2BC9 was observed across various malignant tumor tissues, suggesting that H2BC9 may be involved in tumor initiation and progression (Fig. 2d). Subsequently, the area under the curve (AUC) values for the 1-year, 3-year, and 5-year survival rates of ESCC patients were 0.529, 0.679, and 0.714, respectively, indicating a strong prognostic capability of H2BC9 (Fig. 2e). Similarly, high expression of H2BC9 is associated with poor overall survival (OS) and disease-specific survival (DSS) in ESCC patients (Fig. 2f and g). Furthermore, a clinical prognostic nomogram was constructed for ESCC patients by combining H2BC9 expression levels and pathological stages to predict 1-year, 3-year, and 5-year overall survival (Fig. 2h). Calibration curves were used to validate the model's performance, demonstrating that the model has strong predictive accuracy (Fig. 2i).

The potential biological functions of H2BC9, drug sensitivity predictions, and somatic mutation analysis

To comprehensively investigate the biological functions of H2BC9, correlation analysis was conducted to identify the top 50 genes positively and negatively correlated with its expression (supplement). Protein–protein interaction (PPI) network analysis revealed significant interactions among these genes, providing insights into their functional interconnectivity (Fig. 3a and b). GO and

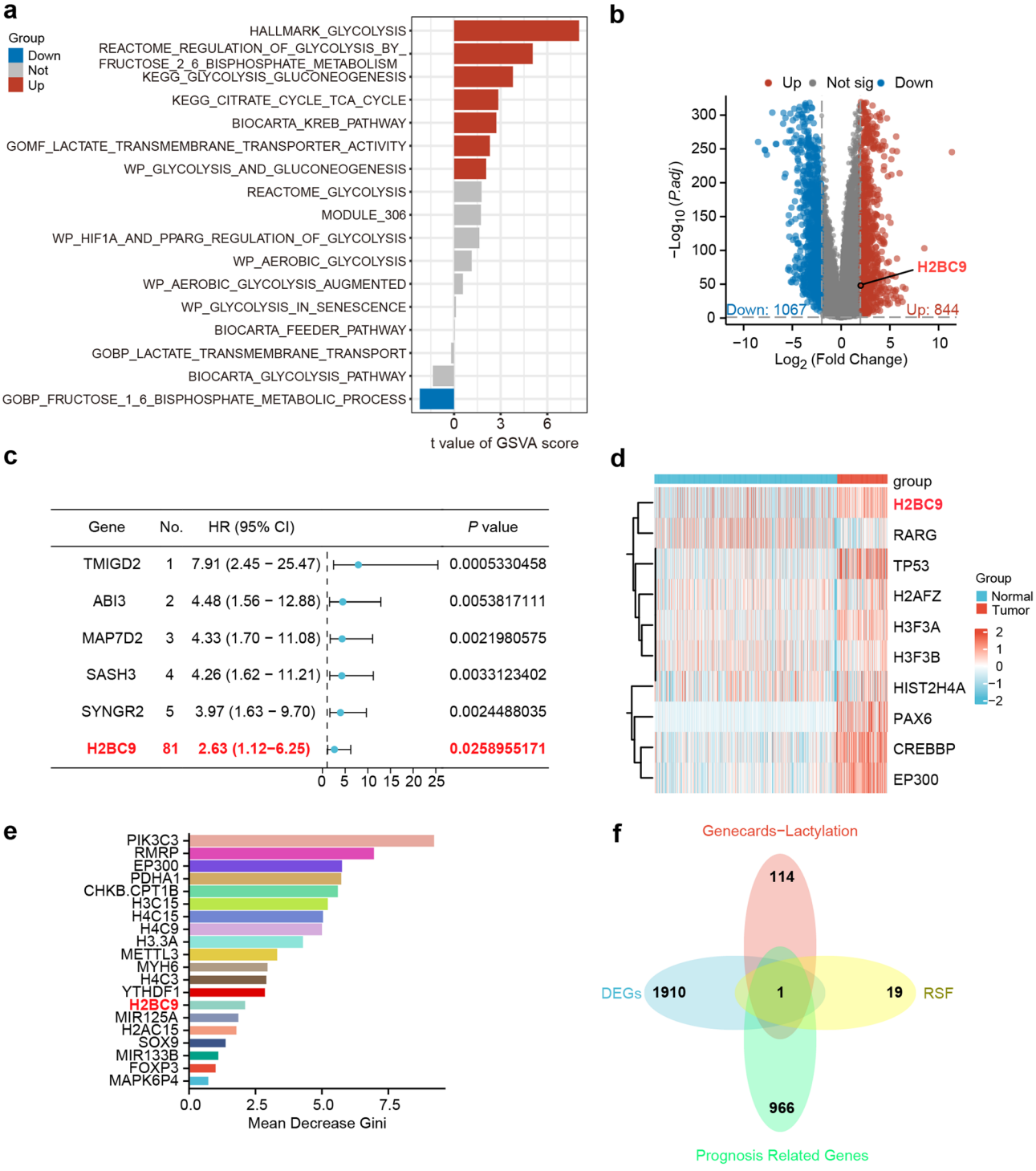

Fig. 1 H2BC9 is a lactate-associated key gene in ESCC. **a**. Differential analysis of the glycolysis metabolic pathway between ESCC tumor tissues and adjacent normal tissues using GSVA. **b**. Identification of differentially expressed genes between ESCC tumor and adjacent normal tissues via the Limma package. **c**. Prognostic genes in ESCC screened by univariate Cox regression analysis. **d**. Heatmap displaying the expression patterns of the top 10 lactate-related genes in ESCC tumor tissues versus adjacent normal tissues. **e**. Signature genes in ESCC revealed by the random forest algorithm. **f**. Venn diagram illustrating the intersection of results from the four analytical approaches

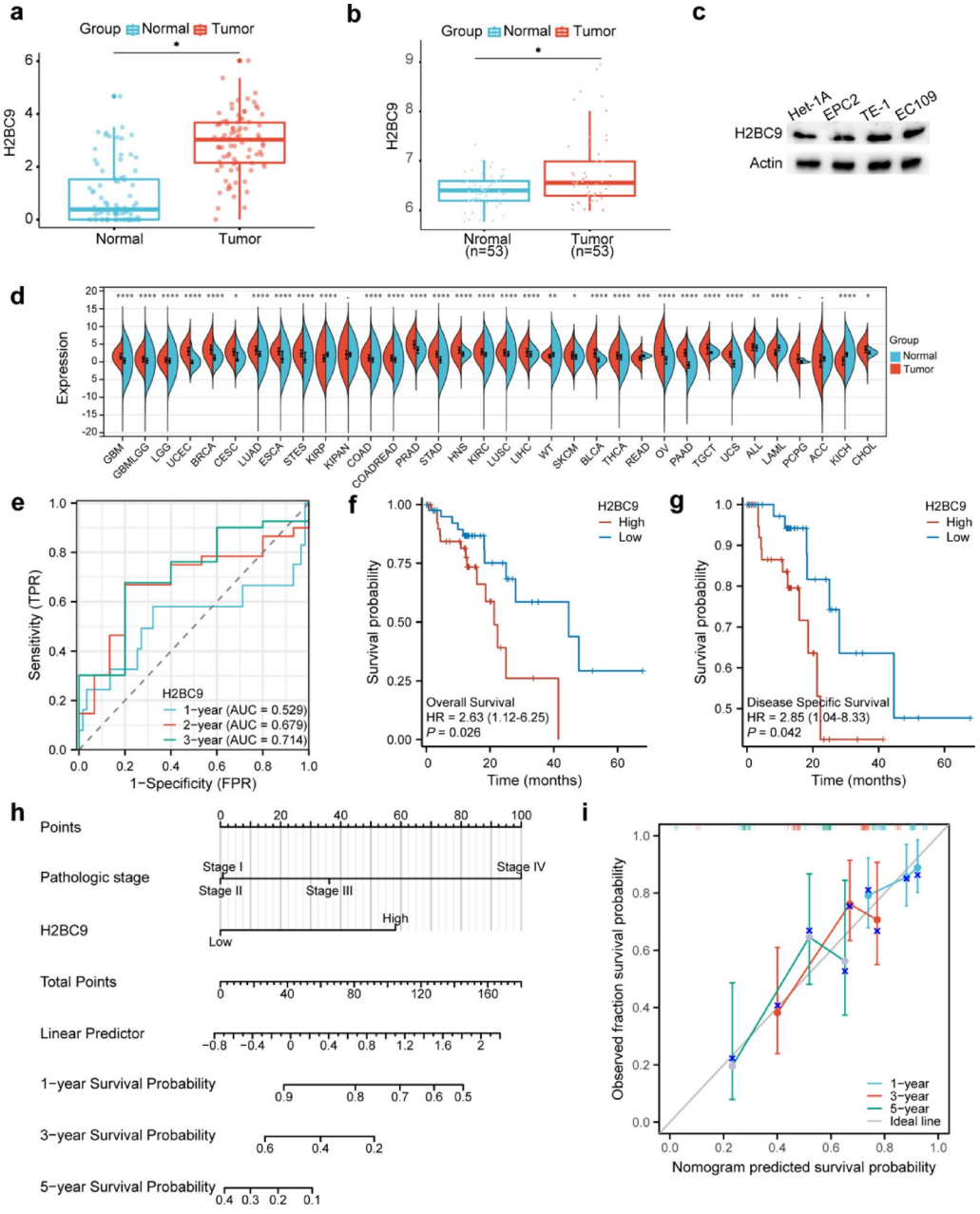

Fig. 2 Expression analysis, survival analysis, and prognostic model construction of H2BC9 in ESCC. **a**. Comparison of H2BC9 expression levels between ESCC tumor tissues and adjacent normal tissues using TCGA database. **b**. Validation of H2BC9 expression differences between ESCC tumor and adjacent normal tissues via GEO database. **c**. WB analysis showing elevated H2BC9 protein expression in ESCC cell lines compared to normal esophageal epithelial cells. **d**. Pan-cancer analysis of H2BC9 expression differences between tumor tissues and matched normal tissues. **e**. Receiver operating characteristic (ROC) curve evaluating the diagnostic value of H2BC9. **f** and **g**. Kaplan–Meier survival analysis demonstrating worse overall survival (OS) and disease-specific survival (DSS) in ESCC patients with high H2BC9 expression. **h**. Nomogram integrating H2BC9 expression levels and clinical characteristics for diagnostic model construction. **i**. Calibration curves assessing the predictive accuracy of the prognostic model

KEGG enrichment analyses indicated that positively correlated genes were primarily involved in processes such as protein-DNA complex assembly and Transcriptional misregulation in cancer, while negatively correlated genes were associated with regulatory functions and cellular signaling (Fig. 3c and d). The relationship between H2BC9 expression and chemotherapeutic sensitivity was further explored using the OncoPredict package (Fig. 3e). Among various chemotherapeutic agents analyzed, paclitaxel demonstrated the most substantial inhibitory effect on ESCC cells. Notably, high H2BC9 expression was associated with reduced sensitivity to paclitaxel. This observation was experimentally validated through CCK8 assays, which revealed a significant decrease in the IC50

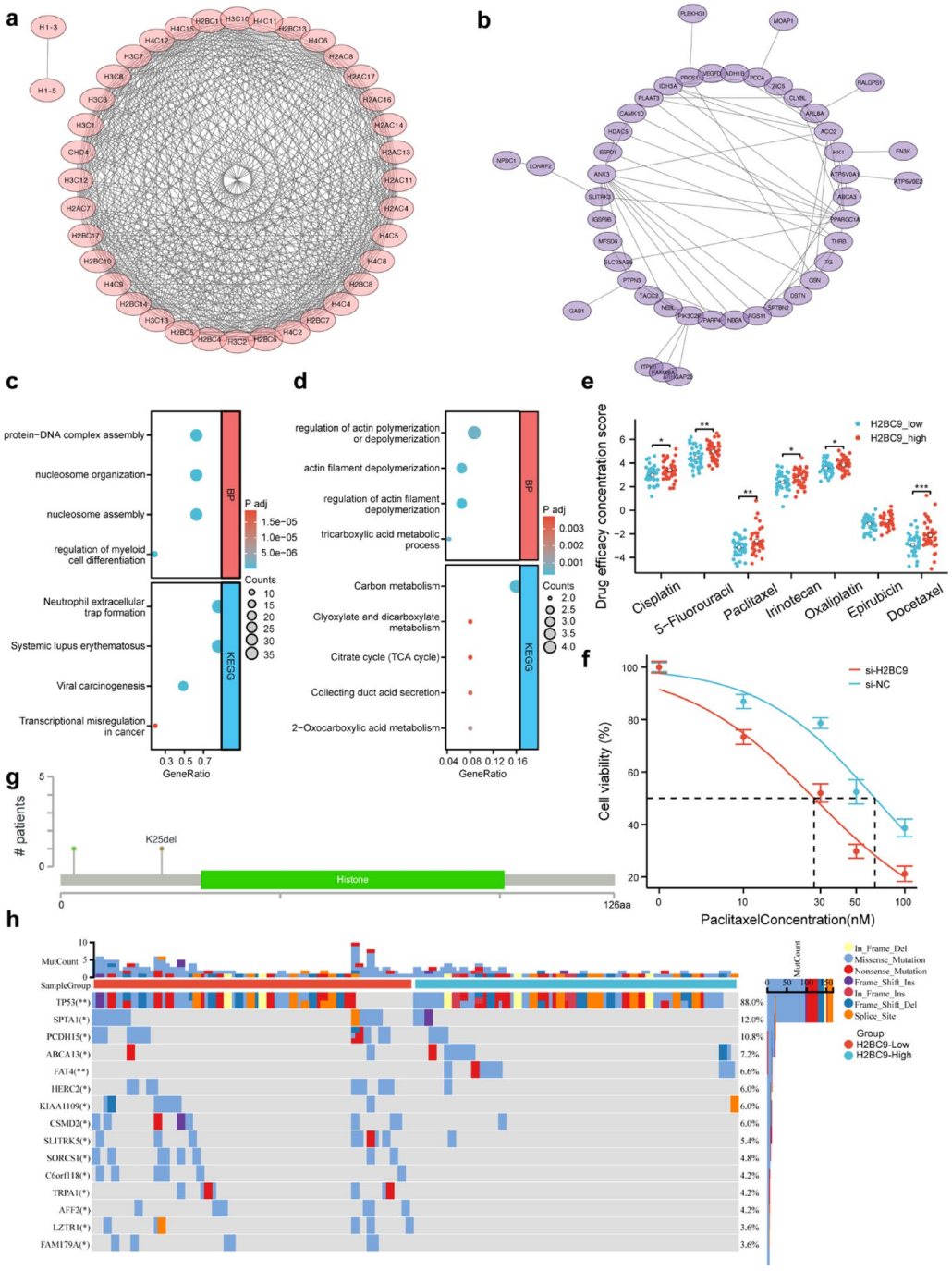

Fig. 3 Bioinformatics prediction of potential functional roles of H2BC9. **a**. Protein–protein interaction (PPI) network of the top 50 genes positively co-expressed with H2BC9. **b**. PPI network of the top 50 genes negatively co-expressed with H2BC9. **c**. GO and KEGG enrichment analyses of the top 50 genes positively correlated with H2BC9 expression. **d**. GO and KEGG enrichment analyses of the top 50 genes negatively correlated with H2BC9 expression. **e**. Prediction of the relationship between H2BC9 expression and chemotherapy sensitivity using the OncoPredict algorithm. **f**. CCK-8 assay demonstrating enhanced paclitaxel sensitivity in ESCC cells following H2BC9 knockdown. **g**. Analysis of H2BC9 mutation hotspots. h. Somatic mutation analysis exploring the association between H2BC9 expression and oncogenic mutation frequency

of paclitaxel following H2BC9 knockdown, suggesting that silencing H2BC9 is associated with increased ESCC cell sensitivity to paclitaxel (Fig. 3f). To gain a deeper understanding of these associations, potential mutation sites and mutation types of H2BC9 were analyzed using cBioPortal (Fig. 3g). Furthermore, the link between H2BC9 expression and the gene mutation landscape was examined. High H2BC9 expression levels were associated with a significantly increased frequency of mutations in cancer-related genes (Fig. 3h). These findings provided

detailed insights into specific mutation patterns that may underpin the functional role of H2BC9 in ESCC pathogenesis, offering valuable directions for future research.

The correlation between H2BC9 expression and the immune microenvironment in ESCC

The relationship between H2BC9 expression and the immune microenvironment in esophageal squamous cell carcinoma (ESCC) was systematically evaluated using CIBERSORT and ssGSEA algorithms, revealing distinct correlations with multiple immune cell populations (Fig. 4a, b). Notably, H2BC9 expression exhibited a significant negative correlation with NK cells and neutrophils, whereas a positive correlation was observed with regulatory T cells (Tregs), activated macrophages (M1 and M0), and activated mast cells.

Analysis of immune cell proportions further demonstrated that high H2BC9 expression was associated with an increased proportion of Tregs and activated macrophages, accompanied by reduced infiltration of $CD8^+$ T cells and NK cells (Fig. 4c). Consistently, Treg enrichment scores calculated by the CIBERSORT algorithm were

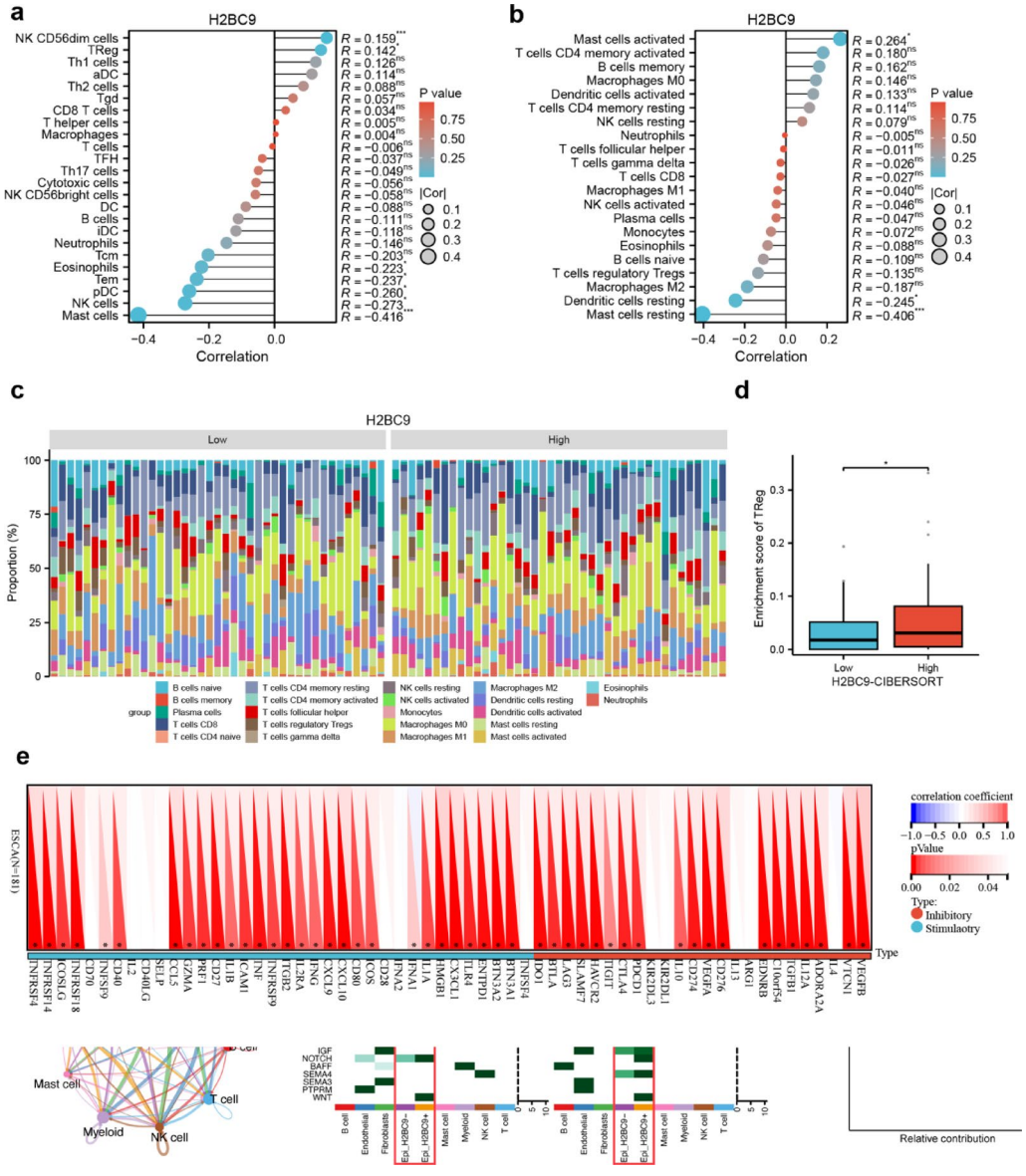

Fig. 4 Association of H2BC9 expression with the immune microenvironment in ESCC. **a**. Correlation between H2BC9 expression and immune cell infiltration levels in ESCC, as assessed by the CIBERSORT algorithm. **b**. Correlation between H2BC9 expression and immune cell infiltration levels, as assessed by the ssGSEA algorithm. **c**. Proportional composition of 22 immune cell subsets in ESCC samples with low and high H2BC9 expression, determined by the CIBERSORT algorithm. **d**. Enrichment scores of regulatory T cells (Tregs) in low and high H2BC9 expression groups, showing a significant increase in Treg infiltration in the high-expression group. **e**. Correlation between H2BC9 expression and immune regulatory genes, with functional annotation of stimulatory or inhibitory roles

significantly higher in the high H2BC9 expression group compared with the low-expression group (Fig. 4d), further supporting the association between H2BC9 and an immunosuppressive cellular milieu.

Moreover, correlation analysis between H2BC9 expression and immune regulatory genes revealed a significant positive association with multiple immune checkpoint molecules, including PDCD1 (PD-1), CTLA4, TIGIT, and LAG3 (Fig. 4e). Many of these genes are known to mediate immune tolerance and T cell exhaustion, suggesting that H2BC9 may contribute to immune evasion through upregulation of inhibitory immune checkpoint pathways.Collectively, these findings indicate that elevated H2BC9 expression is linked to an immunosuppressive tumor microenvironment characterized by increased Treg infiltration and immune checkpoint activation, which may facilitate immune escape and promote ESCC progression.

Analyze the potential functions and pathways of H2BC9 at the single-cell level

In this study, 6 ESCC tissue samples from 5 patients were obtained from the GEO database for comprehensive analysis. UMAP dimensionality reduction and clustering identified eight distinct cell types, including epithelial cells (Fig. 5a–c). These epithelial cells were further categorized into two subgroups based on H2BC9 expression levels. Differential expression analysis between the subgroups revealed 271 upregulated and 59 downregulated genes, which were subsequently subjected to GO and KEGG enrichment analyses (Fig. 5d). The results demonstrated that these differentially expressed genes are predominantly involved in biological processes including cell cycle regulation, the p53 signaling pathway, and cytotoxicity mechanisms (Fig. 5e–f).

To investigate the pathways influenced by H2BC9, intercellular communication patterns were analyzed using CellChat. This analysis uncovered significant differences in signaling activity between the H2BC9-positive and H2BC9-negative epithelial subgroups. Notably, the Wnt/β-catenin signaling pathway was exclusively active in the H2BC9-positive subgroup, implicating H2BC9 as a potential upstream regulator. Further receptor-ligand interaction analysis identified Wnt7b as a key downstream effector within the H2BC9-associated Wnt/β-catenin axis, providing mechanistic insight into the role of H2BC9 in ESCC pathogenesis (Fig. 5g–j).

To assess the diagnostic value of H2BC9, time-dependent ROC analysis was performed. The AUC values for 1-, 3-, and 5-year overall survival prediction were 0.529, 0.679, and 0.714, respectively, suggesting limited short-term predictive power but moderate prognostic potential over longer follow-up periods. These findings indicate that H2BC9 may serve as a biomarker for patient stratification and risk assessment in ESCC.

H2BC9 promotes the activity of the Wnt/β-catenin signaling pathway through increased lactylation and facilitates ESCC tumor growth in vivo

Lactate exposure increased global protein lactylation in a dose-dependent manner, with 25 mM identified as the optimal concentration (Fig. 6a). IP confirmed enhanced lactylation of H2BC9 under this condition (Fig. 6b). Functional assays showed that lactate promoted ESCC cell proliferation, which was significantly suppressed upon H2BC9 knockdown (Fig. 6c, d). Western blot analysis revealed that lactate-induced activation of the Wnt7b/β-catenin pathway depended on H2BC9 expression, suggesting a mechanistic link (Fig. 6e). Notably, treatment with 2-DG reduced H2BC9 lactylation and Wnt/β-catenin activity without altering total H2BC9 protein levels (Fig. 6f), indicating that its lactylation rather than expression drives downstream signaling.

To further validate the pro-tumorigenic role of H2BC9, we established a xenograft model using TE-1 cells with CRISPR-mediated H2BC9 knockout. Tumors derived from sgH2BC9 cells showed significantly reduced growth and weight compared to controls (Fig. 6g–i). These in vivo findings confirm that H2BC9 promotes ESCC progression, at least in part through lactate-driven lactylation and activation of oncogenic signaling pathways.

H2BC9 K44 lactylation is required for Wnt7b transcriptional activation and ESCC tumor progression

To identify the functional lactylation site(s) on H2BC9, TE-1 cells were treated with 25 mM lactate for 24 h, followed by mass spectrometry analysis. Seven candidate lactylation sites were identified (K35, K44, K47, K58, K86, K109, and K117). Integrative prediction using Deep-Kla and FSL-Kla databases further supported K44 as the most conserved and likely functional site (Fig. 7a–b). Structural modeling of H2BC9 K44 and generation of a lysine-to-arginine mutant (K44R) were performed (Fig. 7c), and CRISPR-mediated H2BC9 knockout was followed by reconstitution with either wild-type or mutant constructs.

IP and WB confirmed that the K44R mutant lost its lactylation under high-lactate conditions, while total H2BC9 protein levels remained unchanged (Fig. 7d). Functional assays demonstrated that the K44R mutant failed to promote ESCC cell proliferation, as shown by CCK-8 and colony formation assays (Fig. 7e–f). Moreover, western blot analysis revealed that K44R mutation abolished Wnt7b and β-catenin upregulation in response to lactate (Fig. 7g), consistent with dual-luciferase reporter assays showing impaired Wnt7b promoter activity (Fig. 7h).

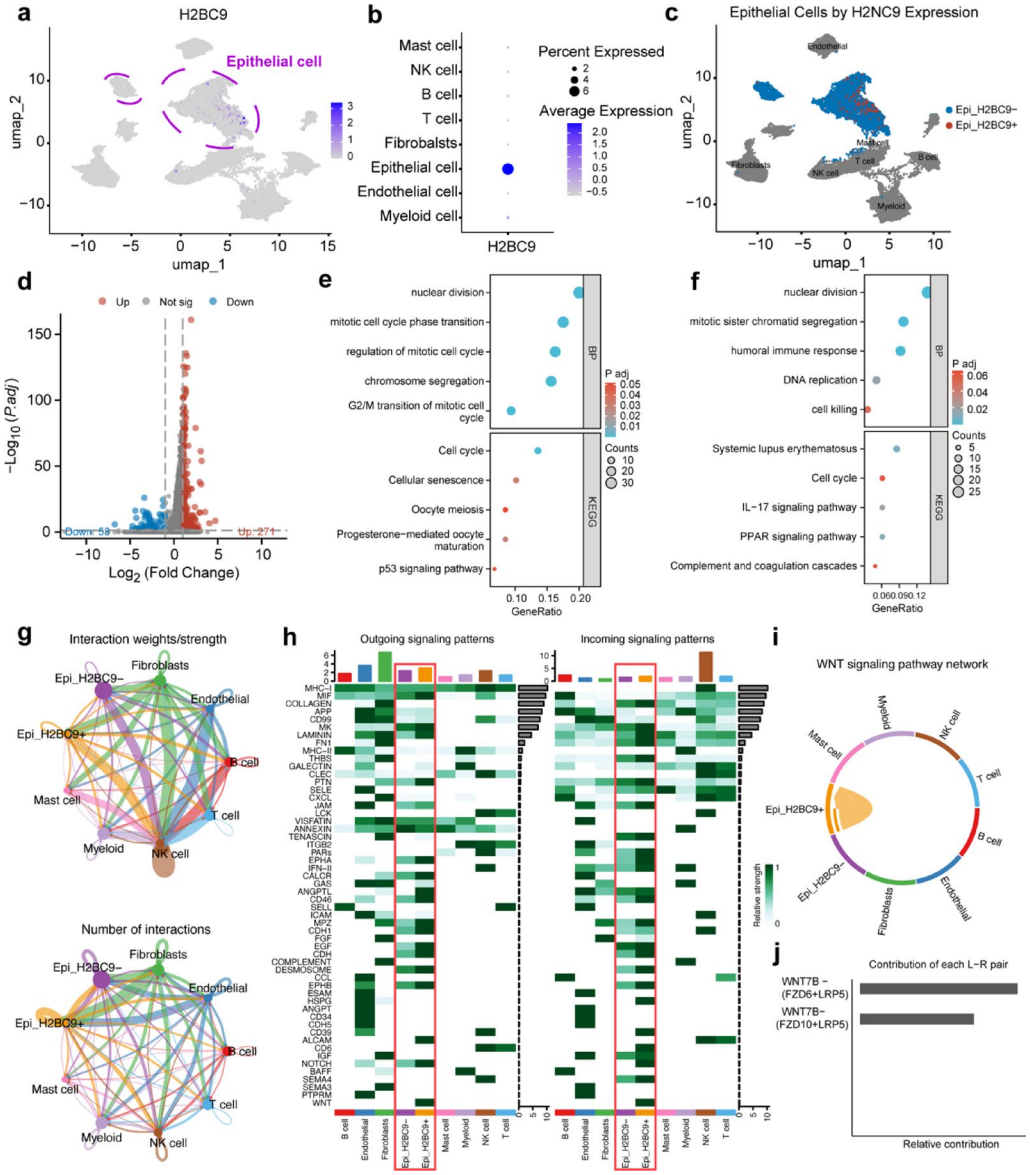

Fig. 5 Single-cell level analysis of H2BC9 expression distribution, function, and potential signaling pathways. **a** and **b**. The expression pattern of H2BC9 across different cell clusters. **c**. The epithelial cell cluster was divided into two groups based on the presence or absence of H2BC9 expression. **d**. A volcano plot illustrating the differentially expressed genes between the two groups. **e** and **f**. GO and KEGG enrichment analyses of the differentially expressed genes between the two groups. **g**–**j**. CellChat analysis comparing the differences in cell–cell communication patterns between H2BC9-expressing and non-expressing epithelial cells

To further verify the transcriptional regulation, ChIP-qPCR analysis demonstrated that wild-type H2BC9 was enriched at the Wnt7b promoter under lactate stimulation, whereas K44R-mutant binding was significantly reduced (Fig. 7i). Additionally, a multi-site mutant (multiKR) in which all lactylation sites except K44 were mutated retained the ability to activate Wnt7b expression (Fig. 7j), supporting the dominant role of K44 lactylation.

In vivo, xenograft assays confirmed that TE-1 cells expressing the K44R mutant failed to form large tumors, as evidenced by reduced tumor volume and weight compared to wild-type H2BC9-expressing cells (Fig. 7k–m). A working model is illustrated in Fig. 7n: lactate-induced H2BC9 K44 lactylation enhances Wnt7b transcription, thereby activating Wnt/β-catenin signaling and promoting ESCC tumor proliferation.

Discussion

ESCC remains a formidable clinical challenge due to its aggressive nature and poor prognosis [24, 25]. While lactate was historically viewed as a metabolic byproduct of glycolysis, recent findings have illuminated its role in epigenetic regulation via protein lactylation [26–29]. In this context, our study highlights the previously unrecognized

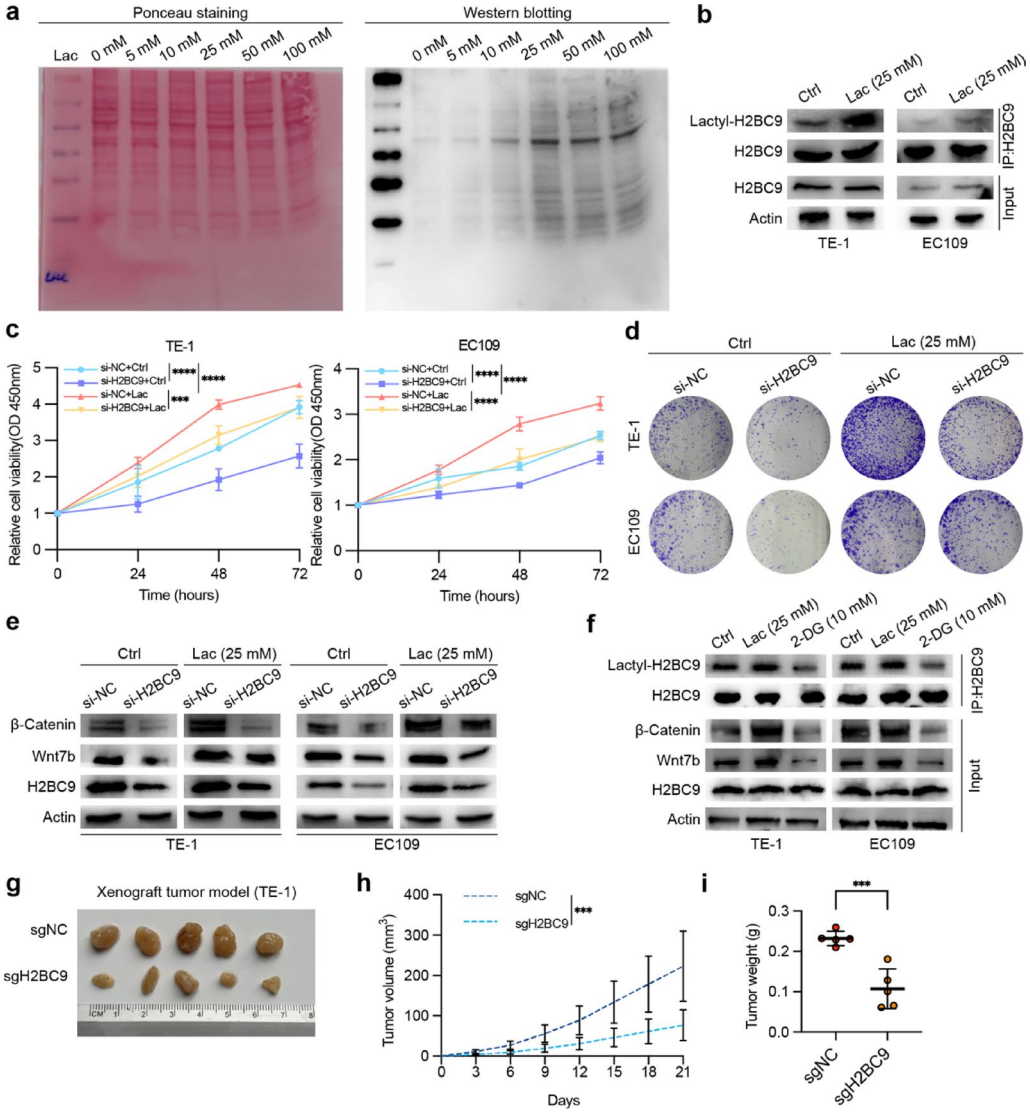

Fig. 6 H2BC9 lactylation promotes ESCC progression through Wnt/β-catenin signaling both in vitro and in vivo.**a**. Ponceau staining and Western blot showing global protein lactylation in TE-1 and EC109 cells treated with increasing concentrations of lactate (0–100 mM). **b**. Immunoprecipitation followed by Western blot confirming enhanced lactylation of H2BC9 in response to 25 mM lactate treatment. **c**–**d**. CCK-8 and colony formation assays showing that H2BC9 knockdown suppresses lactate-induced proliferation in ESCC cells. **e**. Western blot analysis indicating that H2BC9 silencing reduces Wnt7b and β-catenin expression under lactate exposure. **f**. Treatment with the glycolysis inhibitor 2-deoxyglucose (2-DG, 10 mM) attenuates lactate-induced H2BC9 lactylation and downstream Wnt/β-catenin signaling. g. Representative images of xenograft tumors formed by TE-1 cells expressing sgNC or sgH2BC9 in BALB/c nude mice. **h**. Tumor growth curves over 21 days reveal that H2BC9 depletion significantly inhibits tumor progression (n = 5 mice per group). **i**. Tumor weights measured at day 21 confirm a significant reduction in tumor burden in the sgH2BC9 group. Data are presented as mean ± SD. Statistical significance was assessed by unpaired two-tailed Student's t-test (i) and two-way ANOVA with Bonferroni post hoc test (h). Significance levels: ns, not significant; $^{*}P < 0.05$; $^{**}P < 0.01$; $^{***}P < 0.001$; $^{***}P < 0.0001$

oncogenic function of H2BC9, a histone H2B variant, in ESCC progression.

Accumulating evidence indicates that lactate serves as more than a metabolic waste product—it also acts as a key signaling molecule and metabolic substrate within the tumor microenvironment [30, 31]. Tumor-derived lactate contributes to acidosis, immune suppression, angiogenesis, and even metabolic crosstalk between cancer cells and stromal populations [32, 33]. Moreover, intracellular lactate can directly fuel the TCA cycle or act as a donor for post-translational modifications such as histone lactylation, thereby integrating metabolic cues with chromatin regulation [33]. These multifaceted roles of lactate underscore its importance as both a metabolic effector and an epigenetic modulator in cancer biology [34, 35].

By integrating bulk and single-cell transcriptomic analyses with functional and mechanistic validation, we

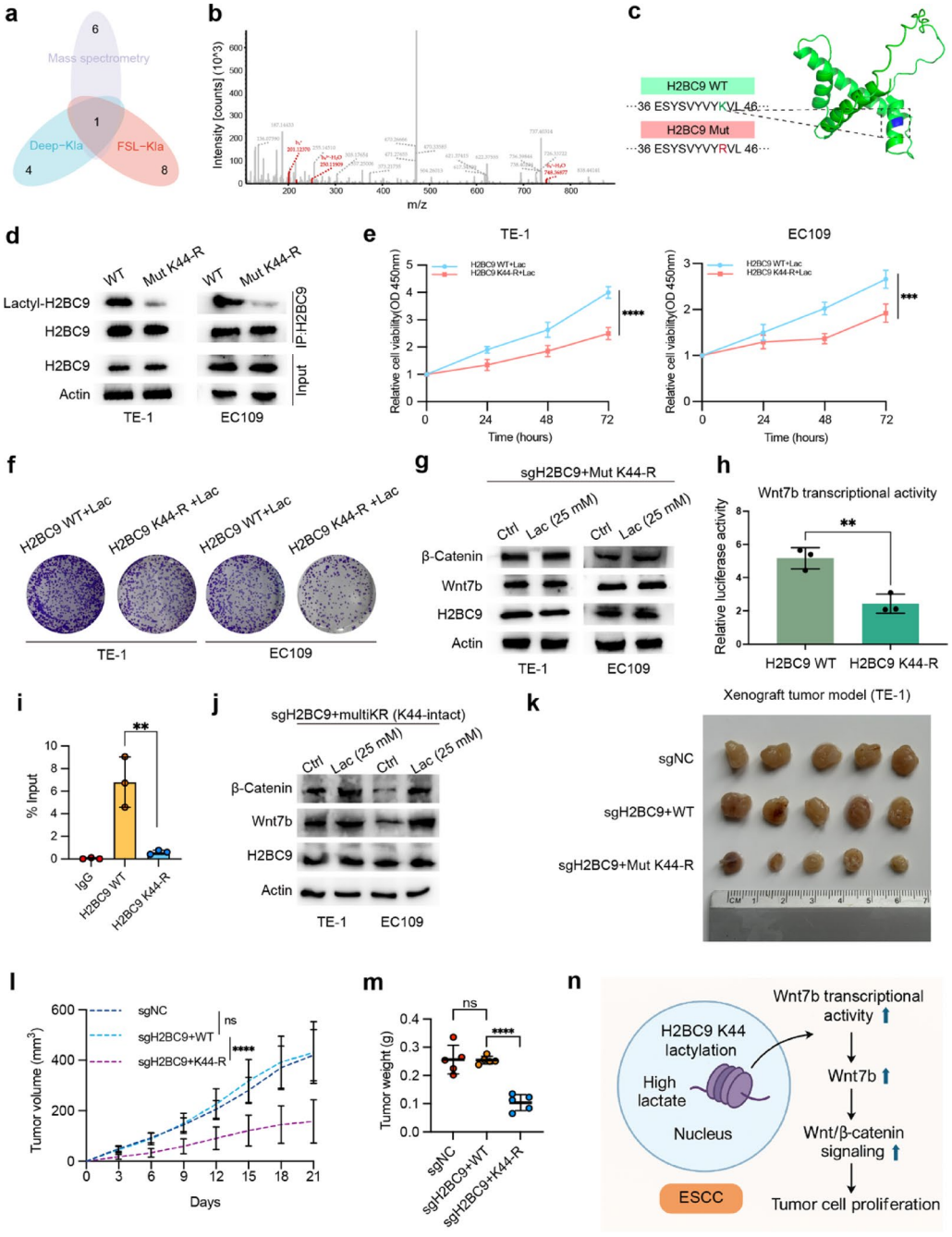

Fig. 7 H2BC9 K44 lactylation is essential for Wnt7b transcriptional activation and ESCC tumor progression. **a**. Venn diagram summarizing potential H2BC9 lactylation sites identified by mass spectrometry and predicted using Deep-Kla and FSL-Kla databases. **b**. MS/MS spectrum validating lysine 44 (K44) lactylation of H2BC9. **c**. Schematic and 3D structural representation of the K44 to R44 mutation (K44R) in H2BC9. **d**. Immunoprecipitation followed by Western blot (IP-WB) shows that the K44R mutant abolishes H2BC9 lactylation. **e**–**f**. CCK-8 and colony formation assays reveal that K44R-mutant H2BC9 fails to rescue proliferation under lactate-rich conditions in ESCC cells. **g**. Western blot showing that the K44R mutant is unable to activate Wnt/β-catenin signaling or upregulate Wnt7b expression. **h**. Dual-luciferase reporter assays show significantly reduced Wnt7b promoter activity in cells expressing the K44R mutant. **i**. ChIP-qPCR analysis confirms reduced recruitment of the K44R mutant to the Wnt7b promoter region. **j**. A multi-site lysine mutant (multiKR), retaining only intact K44, restores responsiveness to lactate and Wnt7b expression. **k**–**m**. Xenograft assays demonstrate that the tumor-promoting function of H2BC9 is abrogated in the K44R mutant group, with reduced tumor volume (l) and weight (m). **n**. Proposed model illustrating that H2BC9 K44 lactylation enhances Wnt7b transcription, thereby promoting Wnt/β-catenin signaling and ESCC cell proliferation. Data are presented as mean ± SD. Statistical significance was determined by two-way ANOVA with Bonferroni post hoc test (l), and unpaired two-tailed Student's t-test (h, i, m). Significance levels: ns, not significant; *$P < 0.05$; **$P < 0.01$; ***$P < 0.001$; ***$P < 0.0001$

identified H2BC9 as a lactylation-associated gene highly expressed in ESCC. Notably, lactate-induced K44 lactylation of H2BC9 modulates transcriptional activity of Wnt7b, thereby influencing the Wnt/β-catenin signaling axis—a pathway long implicated in tumorigenesis. Functional assays and luciferase reporter experiments support the hypothesis that H2BC9 acts as a lactylation-responsive chromatin modulator [36].

Furthermore, the association of H2BC9 with immune evasion and chemotherapeutic resistance underscores its translational relevance. Elevated H2BC9 expression correlated with immunosuppressive microenvironment features, including Treg enrichment and checkpoint gene expression, suggesting a potential role in modulating anti-tumor immunity. Sensitization of ESCC cells to paclitaxel upon H2BC9 knockdown also points to its utility as a predictive biomarker for therapy response.

Compared to prior studies focusing predominantly on histone H3, our work emphasizes the underexplored yet significant role of H2B family members in cancer epigenetics [15, 16, 37]. These findings expand the functional repertoire of histone lactylation and propose H2BC9 as both a mechanistic driver and a candidate therapeutic target in ESCC.

Nonetheless, limitations remain. While K44 was validated as a key lactylation site, other potential sites require further functional validation. Additionally, the enzymes responsible for H2BC9 lactylation and delactylation remain to be identified. Future investigations should aim to elucidate these regulatory mechanisms and explore broader implications across cancer types.

In summary, our study provides a novel mechanistic link between lactate metabolism, histone lactylation, and oncogenic signaling in ESCC. Targeting H2BC9 lactylation may represent a promising strategy to overcome therapeutic resistance and reshape the tumor microenvironment.

Conclusion

H2BC9 is overexpressed in ESCC and correlates with poor patient prognosis, as well as heightened sensitivity to docetaxel, positioning it as a potential biomarker for diagnosis and prognosis. Under lactate-induced conditions, K44 of H2BC9 is lactylated, facilitating ESCC cell proliferation and enhancing Wnt7b transcriptional activity. This, in turn, is linked to increased Wnt/β-catenin signaling activity and the oncogenic potential of H2BC9.

Abbreviations

β-catenin	Beta-catenin
CCK-8	Cell counting Kit-8
CIBERSORT	Cell-type identification by estimating relative subsets of RNA transcripts
CRISPR	Clustered regularly interspaced short palindromic repeats
CTLA-4	Cytotoxic T-lymphocyte associated protein 4
DSS	Disease-specific survival
EC	Esophageal cancer
ECL	Enhanced chemiluminescence
ESCC	Esophageal squamous cell carcinoma
FDR	False discovery rate
GEO	Gene expression omnibus
GO	Gene ontology
GSVA	Gene set variation analysis
GTEx	Genotype-tissue expression
HRP	Horseradish peroxidase
IC50	Half maximal inhibitory concentration
IP	Immunoprecipitation
KEGG	Kyoto encyclopedia of genes and genomes
KM	Kaplan–Meier
LC–MS/MS	Liquid chromatography-tandem mass spectrometry
MSigDB	Molecular signatures database
OS	Overall Survival
Paclitaxel	A microtubule-stabilizing chemotherapeutic agent
PPI	Protein–Protein Interaction
qRT-PCR	Quantitative reverse transcription polymerase chain reaction
RNA-seq	RNA sequencing
ROC	Receiver operating characteristic
scRNA-seq	Single-cell RNA sequencing
STRING	Search tool for the retrieval of interacting genes/proteins
TCGA	The cancer genome atlas
Treg	Regulatory T cell
WB	Western blot
Wnt7b	Wingless-type MMTV integration site family member 7B

Supplementary Information

The online version contains supplementary material available at https://doi.org/10.1186/s12967-025-07144-4.

Additional file1

Additional file2

Acknowledgements

We extend our thanks to the TCGA and GEO databases for providing a wealth of sample sequencing information.

Author contributions

Yuxiang Zhang, Ce shi and Yun Zhou contributed equally to this manuscript. Dongsheng Pei and Jie Mou designed this study. Yuxiang Zhang and Ce Shi in vitro experiments, drafted and revised the manuscript. Yun Zhou completed the bioinformatics. Jing Zhu and Keke Xia participated in the statistical analysis of in vitro experiments. The article has been revised by the Lansheng Zhang. All authors approved this manuscript.

Funding

This work was supported by National Natural Science Foundation of China (82273160), The Youth Medical Science and Technology Innovation Project of Xuzhou Municipal Health Commission (XWKYHT20210565), and Development Fund Sponsored Projects of the Affiliated Hospital of Xuzhou Medical University (XYFM202235).

Availability of data and materials

The datasets during and/or analysed during the current study available from the corresponding author on reasonable request. ScRNA-seq data are downloaded at https://www.ncbi.nlm.nih.gov/geo/query/acc.cgi?acc=GSE188900. Bulk RNA-seq data were downloaded from the TCGA database. Data is provided within the manuscript or supplementary information files.

Declarations

Ethics approval and consent to participate

Not applicable.

Consent for publication

Not applicable.

Competing interests
The authors declare that they have no competing interests.

Clinical trial number
Not applicable.

Author details
[1]Department of Pathology, School of Basic Medical Sciences, Xuzhou Medical University, 209 Tongshan Road, Xuzhou 221004, Jiangsu, People's Republic of China
[2]Department of Oncological Radiotherapy, The Second Affiliated Hospital of Xuzhou Medical University, 32 Meijian Road, Xuzhou 221006, Jiangsu, People's Republic of China
[3]School of Pharmacy, Xuzhou Medical University, Xuzhou, People's Republic of China
[4]Nanjing Drum Tower Hospital and Group's Suqian Hospital, Affiliated Hospital of Medical School, Nanjing University, Xuzhou, People's Republic of China
[5]Department of Radiotherapy, XuZhou Clinical School of Xuzhou Medical University, Xuzhou, People's Republic of China
[6]The Municipal Hospital Affiliated to Xuzhou Medical University, Xuzhou, People's Republic of China

Received: 27 June 2025 / Accepted: 11 September 2025
Published online: 14 October 2025

References

1. GK Malhotra U Yanala A Ravipati M Follet M Vijayakumar C Are 2017 Global trends in esophageal cancer J Surg Oncol 115 5 564 579 https://doi.org/10.1002/JSO.24592
2. E Morgan I Soerjomataram H Rumgay 2022 The global landscape of esophageal squamous cell carcinoma and esophageal adenocarcinoma incidence and mortality in 2020 and projections to 2040: new estimates from GLOBOCAN 2020 Gastroenterology 163 3 649 658.e2 https://doi.org/10.1053/J.GASTRO.2022.05.054
3. B Han R Zheng H Zeng 2024 Cancer incidence and mortality in China, 2022 J Natl Cancer Center https://doi.org/10.1016/J.JNCC.2024.01.006
4. S He J Xu X Liu Y Zhen 2021 Advances and challenges in the treatment of esophageal cancer Acta Pharm Sin B 11 11 3379 3392 https://doi.org/10.1016/J.APSB.2021.03.008
5. H Liu S Wang J Wang 2025 Energy metabolism in health and diseases Signal Transduct Target Ther 10 1 69 https://doi.org/10.1038/S41392-025-02141-X
6. D Hanahan RA Weinberg 2011 Hallmarks of cancer: the next generation Cell 144 5 646 674 https://doi.org/10.1016/J.CELL.2011.02.013
7. GJ Yoshida 2015 Metabolic reprogramming: the emerging concept and associated therapeutic strategies J Exp Clin Cancer Res 34 1 111 https://doi.org/10.1186/S13046-015-0221-Y
8. X Wang L Wang Q Hao M Cai X Wang W An 2024 Harnessing glucose metabolism with nanomedicine for cancer treatment Theranostics 14 17 6831 6882 https://doi.org/10.7150/THNO.100036
9. M Martino De JC Rathmell L Galluzzi C Vanpouille-Box 2024 Cancer cell metabolism and antitumour immunity Nat Rev Immunol 24 9 654 669 https://doi.org/10.1038/S41577-024-01026-4
10. H Hefzi I Martínez-Monge I Marin de Mas NL Cowie AG Toledo SM Noh KJ Karottki M Decker J Arnsdorf JM Camacho-Zaragoza S Kol 2025 Multiplex genome editing eliminates lactate production without impacting growth rate in mammalian cells Nature Metab 7 1 212 227 https://doi.org/10.1038/S42255-024-01193-7
11. J Huang H Xie J Li 2025 Histone lactylation drives liver cancer metastasis by facilitating NSF1-mediated ferroptosis resistance after microwave ablation Redox Biol 81 103553 https://doi.org/10.1016/J.REDOX.2025.103553
12. X Li Y Yang B Zhang 2022 Lactate metabolism in human health and disease Signal Transduct Target Ther https://doi.org/10.1038/S41392-022-01151-3
13. J Chen Z Huang Y Chen 2025 Lactate and lactylation in cancer Signal Transduct Target Ther 10 1 38 https://doi.org/10.1038/S41392-024-02082-X
14. D Zhang Z Tang H Huang 2019 Metabolic regulation of gene expression by histone lactylation Nature 574 7779 575 580 https://doi.org/10.1038/S41586-019-1678-1
15. J Jia Z Han X Wang X Zheng S Wang Y Cui 2022 H2B gene family: A prognostic biomarker and correlates with immune infiltration in glioma Front Oncol https://doi.org/10.3389/FONC.2022.966817
16. W Zhang X Chen Z Wang 2024 Identification of HIST1H2BH as the hub gene associated with multiple myeloma using integrated bioinformatics analysis Hematology https://doi.org/10.1080/16078454.2024.2335421
17. K Mortezaee 2023 B7–H3 immunoregulatory roles in cancer Biomed Pharmacother https://doi.org/10.1016/J.BIOPHA.2023.114890
18. L Wu L Li M Zhu 2025 Evaluating H2BC9 as a potential diagnostic and prognostic biomarker in head and neck squamous cell carcinoma Eur J Med Res 30 1 54 https://doi.org/10.1186/S40001-025-02301-3
19. H Su H Xue S Gao 2022 Effect of rhizoma drynariae on differential gene expression in ovariectomized rats with osteoporosis based on transcriptome sequencing Front Endocrinol (Lausanne) https://doi.org/10.3389/FENDO.2022.930912
20. D Ray-Gallet G Almouzni 2022 H3–H4 histone chaperones and cancer Curr Opin Genet Dev https://doi.org/10.1016/J.GDE.2022.101900
21. J Yu Y Yan S Li 2024 Progestogen-driven B7–H4 contributes to onco-fetal immune tolerance Cell 187 17 4713 4732.e19 https://doi.org/10.1016/J.CELL.2024.06.012
22. A Subramanian H Kuehn J Gould P Tamayo JP Mesirov 2007 GSEA-P: a desktop application for Gene Set enrichment analysis Bioinformatics 23 23 3251 3253 https://doi.org/10.1093/BIOINFORMATICS/BTM369
23. M Rebhan V Chalifa-Caspi J Prilusky D Lancet 1997 GeneCards: integrating information about genes, proteins and diseases Trends Genet 13 4 163 https://doi.org/10.1016/S0168-9525(97)01103-7
24. JE Rogers M Sewastjanow-Silva RE Waters JA Ajani 2022 Esophageal cancer: emerging therapeutics Expert Opin Ther Targets 26 2 107 117 https://doi.org/10.1080/14728222.2022.2036718
25. N Deboever CM Jones K Yamashita JA Ajani WL Hofstetter 2024 Advances in diagnosis and management of cancer of the esophagus BMJ https://doi.org/10.1136/BMJ-2023-074962
26. H Li L Sun P Gao H Hu 2024 Lactylation in cancer: current understanding and challenges Cancer Cell https://doi.org/10.1016/J.CCELL.2024.09.006
27. S Chen Y Xu W Zhuo L Zhang 2024 The emerging role of lactate in tumor microenvironment and its clinical relevance Cancer Lett https://doi.org/10.1016/J.CANLET.2024.216837
28. H Chen Y Li H Li 2024 NBS1 lactylation is required for efficient DNA repair and chemotherapy resistance Nature 631 8021 663 669 https://doi.org/10.1038/S41586-024-07620-9
29. W Liu Y Wang LHM Bozi 2023 Lactate regulates cell cycle by remodelling the anaphase promoting complex Nature 616 7958 790 797 https://doi.org/10.1038/S41586-023-05939-3
30. W Zhang G Wang ZG Xu 2019 Lactate is a natural suppressor of RLR signaling by targeting MAVS Cell 178 1 176 189.e15 https://doi.org/10.1016/J.CELL.2019.05.003
31. GA Brooks 2018 The science and translation of lactate shuttle theory Cell Metab 27 4 757 785 https://doi.org/10.1016/J.CMET.2018.03.008
32. B Faubert KY Li L Cai 2017 Lactate metabolism in human lung tumors Cell 171 2 358 371.e9 https://doi.org/10.1016/J.CELL.2017.09.019
33. S Hui JM Ghergurovich RJ Morscher C Jang X Teng W Lu LA Esparza T Reya L Zhan J Yanxiang Guo E White 2017 Glucose feeds the TCA cycle via circulating lactate Nature 551 7678 115 118 https://doi.org/10.1038/nature24057
34. P Vaupel H Schmidberger A Mayer 2019 The warburg effect: essential part of metabolic reprogramming and central contributor to cancer progression Int J Radiat Biol 95 7 912 919 https://doi.org/10.1080/09553002.2019.1589653
35. I San-Millán GA Brooks 2017 Reexamining cancer metabolism: lactate production for carcinogenesis could be the purpose and explanation of the Warburg Effect Carcinogenesis 38 2 119 133 https://doi.org/10.1093/CARCIN/BGW127
36. R Nusse H Clevers 2017 Wnt/β-catenin signaling, disease, and emerging therapeutic modalities Cell 169 6 985 999 https://doi.org/10.1016/J.CELL.2017.05.016
37. Z Liu X Zhao R Wang 2023 Heterogeneous pattern of gene expression driven by TTN mutation is involved in the construction of a prognosis model of lung squamous cell carcinoma Front Oncol https://doi.org/10.3389/FONC.2023.916568

Publisher's Note